

1 **Observations and scaling of tidal mass transport across**
2 **the lower Ganges-Brahmaputra delta plain:**
3 **implications for delta management and sustainability**
4

5 Richard Hale¹, Rachel Bain², Steven Goodbred Jr.², Jim Best³

6 ¹Dept. of Ocean, Earth, and Atmos. Sci., Old Dominion University, Norfolk, VA, USA

7 ²Earth and Environmental Sciences Dept., Vanderbilt University, Nashville, TN USA

8 ³Departments of Geology, Geography & GIS, Mechanical Science and Engineering and Ven
9 Te Chow Hydrosystems Laboratory, University of Illinois, Urbana, IL USA

10
11 **Abstract**
12

13 The landscape of southwest Bangladesh, a region constructed primarily by fluvial
14 processes associated with the Ganges and Brahmaputra Rivers, is now maintained almost
15 exclusively by tidal processes as the fluvial system has migrated east and eliminated most
16 direct fluvial input. In natural areas such as the Sundarbans National Forest, year-round
17 inundation during spring high tides delivers sufficient sediment that enables vertical
18 accretion to keep pace with relative sea-level rise. However, recent human modification of
19 the landscape in the form of embankment construction has terminated this pathway of
20 sediment delivery for much of the region, resulting in a startling elevation imbalance, with
21 inhabited areas often sitting >1 m below mean high water. Restoring this landscape, or
22 preventing land loss in the natural system, requires an understanding of how rates of water
23 and sediment flux vary across time scales ranging from hours to months. In this study, we
24 combine time-series observations of water level, salinity, and suspended sediment
25 concentration, with ship-based measurements of large tidal-channel hydrodynamics and
26 sediment transport. To capture the greatest possible range of variability, cross-channel
27 transects designed to encompass a 12.4-h tidal cycle were performed in both dry and wet
28 seasons, during spring and neap tides.
29

30 Regional suspended sediment concentration begins to increase in August, coincident with a
31 decrease in local salinity, indicating the arrival of the sediment-laden, freshwater plume of
32 the combined Ganges-Brahmaputra-Meghna rivers. We observe profound seasonality in
33 sediment transport, despite comparatively modest seasonal variability in the magnitude of
34 water discharge. These observations emphasize the importance of seasonal sediment
35 delivery from the mainstem rivers to this remote tidal region. On tidal time-scales, spring
36 tides transport an order of magnitude more sediment than neap tides in both the wet and
37 dry seasons. In aggregate, sediment transport is flood-oriented, likely a result of tidal
38 pumping. Finally, we note that rates of sediment and water discharge in the tidal channels
39 are of the same scale as the annually averaged values for the Ganges or Brahmaputra
40 rivers. These observations provide context for examining the relative importance of fluvial
41 and tidal processes in what has been defined as a quintessentially tidally influenced delta in
42 the classification scheme of Galloway (1975). These data also inform critical questions
43 regarding the timing and magnitude of sediment delivery to the region, which are
44 especially important in predicting, and preparing for, responses of the natural system to
45 ongoing environmental change.
46

47
48
49
50
51
52
53
54
55
56
57
58
59
60
61
62
63
64
65
66
67
68
69
70
71
72
73
74
75
76
77
78
79
80
81
82
83
84
85
86
87
88
89
90
91

1 – Introduction

The world’s great deltas are currently threatened by a variety of factors, including global sea level rise (Overeem and Syvitski, 2009), overpopulation (Ericson et al., 2006), changes in sediment supply (Syvitski 2003; Syvitski and Milliman, 2007; Anthony et al., 2015; Darby et al., 2016; Best, 2019), and other human-related activities such as water diversions, flood control structures, and groundwater and hydrocarbon extraction (Syvitski et al., 2009). The Ganges-Brahmaputra-Meghna (GBM) delta is one of the most heavily populated regions that is undergoing locally accelerated sea-level rise (~0.5 cm/y; Higgins et al., 2014) due to a combination of natural and anthropogenic factors including eustatic sea-level change, tectonic subsidence, fine-grained sediment compaction, and groundwater extraction (Overeem and Syvitski, 2009; Syvitski, 2008; Steckler et al., 2010). In addition, when factors such as tidal amplification due to anthropogenic reworking of the distributary channel network are considered, the relative rate of sea-level rise can exceed 1.6 cm/yr (Pethick and Orford, 2013). Furthermore, the future viability of the delta is threatened by the proposed construction of dams and water diversions associated with India’s National River Linking Project, which, if completed as proposed, could drastically reduce sediment delivery to Bangladesh (Higgins et al., 2018).

Restoration of land-surface elevation in many populated areas in the GBM delta is already necessary due to the relative loss in elevation that has occurred since the widespread construction of embankments during the 1960s to 1980s. Both planned (tidal river management) and unplanned (embankment failures) flooding of local polders (the embanked islands) has demonstrated the capacity of the natural system for effective sediment transport and deposition, with decimeters of annual accretion observed during recent breach events (Khadim et al., 2013; Auerbach et al., 2015; Kamal et al., 2017; Darby et al., 2018). One of the most important strategies that has been forwarded to reduce the threat of unintended inundations in SW Bangladesh is a plan for polder management (Brammer, 2014). However, many questions concerning potential management strategies remain, not the least of which are an accurate quantification of total available sediment mass and an understanding of the tidal processes involved in its transport and deposition. Toward these goals, the present study provides observation-based calculations of water and sediment transport through a major tidal channel in the delta across spring-neap tidal cycles and seasonal time scales, with the goal of identifying the timing and magnitude of mass sediment exchange between the different tidal channels. Not considered in the present study are the potential impacts of tropical cyclones, which directly impact Bangladesh 0.3-1.5 times per year (Murty et al., 2986; Alam et al., 2003; Saha and Khan, 2014), and can significantly affect the local landscape (Auerbach et al., 2015). The results presented herein are considered in the context of prior research concerning sediment accumulation and rates of channel infilling to better understand the role of tidal mass transport within the lower GBM delta plain.

2 – Background

92 Much of the low-lying coastal region of SW Bangladesh is under threat of long-term
93 inundation (Auerbach et al., 2015; Brown and Nicholls, 2015). The risk is particularly acute
94 for islands that were embanked (“poldered”) in the 1960s and 1970s as part of a program
95 designed to increase the area of arable land through the prevention of tidal inundation in
96 agricultural areas (Islam, 2006; Nowreen et al., 2014). Approximately 5000 km of polder
97 embankments were built by hand, generating 9000 km² of new farmland, but also
98 eliminating the semi-diurnal exchange of water and sediment between the tidal channels
99 and tidal platform (Islam, 2006; Nowreen et al., 2014). As a result, sediment resupply
100 pathways have been effectively terminated and the former floodplain surface in these
101 regions now lies 1.0-1.5 m below mean high water due to a combination of sediment
102 starvation, enhanced compaction, and tidal-range amplification (Auerbach et al., 2015;
103 Pethick and Orford, 2013).

104

105 In contrast to the poldered landscape, the adjacent mangrove system of the Sundarbans
106 National Forest (SNF) is primarily inundated during spring high tides, and its
107 sedimentation and vegetation are keeping pace with sea-level rise (Rogers et al., 2013;
108 Auerbach et al., 2015). Protecting the SNF is of critical importance, as coastal wetlands and
109 mangroves provide irreplaceable ecosystem services including storm-surge buffering
110 (Uddin et al., 2013; Marois and Mitsch, 2015; Hossain et al., 2016; Sakib et al., 2015),
111 serving as effective carbon traps (Mcleod et al., 2011; Alongi, 2012; Pendleton et al., 2012)
112 and perhaps even helping to combat the impacts of ocean acidification (Yan, 2016).

113

114 For the GBM delta, a unit-scale analysis of mass balance (Rogers et al., 2013) suggests that
115 the annual sediment load of the GBM river system (~1.1 Gt/y) is sufficient to aggrade the
116 entire delta system at rates ≥ 0.5 cm/yr, and thus provides potential to keep pace with
117 moderately high rates of sea-level rise. Such aggradation, of course, requires effective
118 dispersal of riverine sediment to disparate regions of the delta. Recent research suggests a
119 close coupling of discharge at the river mouth to sediment deposition in the remote delta
120 plain by way of tidal exchange (Allison and Kepple, 2001; Rogers et al., 2013; Auerbach et
121 al., 2015; Wilson et al., 2017). Such tidally supported sedimentation yields mean accretion
122 rates of ~1 cm/yr, with local observations regularly reaching 3-5 cm/yr, which together
123 indicate robust sediment delivery to the Sundarbans and SW coastal region (Rogers et al.,
124 2013; Rogers and Overeem, 2017). Thus, as the principal conduit for sediment that can
125 maintain the elevation of this region, an understanding and quantification of the tidal water
126 and sediment exchange is essential to foresee future impacts of accelerated sea-level rise
127 and the potential for mitigation.

128

129 **3 – Methods**

130

131 **3.1 – Study Area**

132 Our research concerns a network of tidal channels located approximately 80 km from the
133 coast along the Pussur River system, itself one of five similarly sized tidal distributary
134 networks (Fig. 1). Tidal exchange extends >120 km inland of the coast along the Pussur
135 River, with one branch ultimately connecting to the Gorai River, a distributary of the
136 mainstem Ganges River (Fig. 1). The tidal range along the Pussur River approaches its
137 maximum in the study area at 4-5 m for the spring tidal range, as compared with 3-3.5 m

138 on the coast at Hiron Point. The area is also societally relevant, lying at the transition from
139 the pristine Sundarbans forest to the embanked polders, and near the formerly active
140 shipping port of Mongla and cyclone- and flood- impacted island of Polder 32 (labelled P32
141 on Fig. 1; Auerbach et al., 2015).

142
143 Within this area, our observations were collected in the primary tidal channel of the Shibsa
144 River and two of its major bifurcations that connect with the Pussur channel, the Dhaki
145 River and Bhadra River (Fig. 1). The Shibsa River is the largest of these channels, with local
146 widths of 1-2 km, compared to 0.25-0.8 km and 0.15-0.3 km, for the Dhaki and Bhadra
147 Rivers, respectively. At its eastern extent, the Dhaki River connects to the Pussur River,
148 serving as the first major cross-channel to link the Shibsa and Pussur River channels after
149 they bifurcate ~60 km to the south (Fig. 1). At its upstream extent, the Pussur tidal channel
150 connects with the downstream mouth of the Gorai River, which delivers a water discharge
151 of ~3000 m³/s during the monsoon season and decreasing to ~0 m³/s during the dry
152 season (Winterwerp and Giardino, 2012). Salinity in the study area ranges from 0-1 PSU
153 during the monsoon, to 20-30 PSU during the dry season (Shaha and Cho, 2016; Ayers et
154 al., 2018). This seasonal variation in salinity is controlled by local runoff, freshwater
155 discharge from the Gorai River, and to a much larger extent, the magnitude of the regional
156 discharge plume of the GBM rivers (Rogers et al., 2013).

157 158 **3.2. – Hydrodynamic Observations**

159
160 To establish tidal stage and capture surface-water elevations during the hydrodynamic
161 surveys, pressure sensors were deployed at multiple locations across the study area (Fig.
162 1). All sensors were deployed as close to low water as possible and recorded at 5- or 10-
163 minute intervals. Periods of subaerial sensor exposure (of up to 150 minutes at low tide)
164 were interpolated using a robust ordinary least-squares method provided by Grinsted
165 (2008). The agreement between measurement and prediction was generally good, with
166 predicted range being 0.98 of the measured range for a given time period, thus suggesting
167 that the interpolated data are both reasonable and conservative. The values reported
168 herein are of the interpolated values. Tidal range, water temperature, and conductivity
169 have also been monitored continuously since 2014 at the Sutarkhali station (Fig. 1B), with
170 an optical backscatter sensor (OBS) calibrated to measure suspended sediment
171 concentration (SSC) added in late March 2015. Prior to deployment in the tidal channel,
172 this OBS was used to measure vertical profiles of SSC on the Shibsa River, with
173 simultaneous water samples being collected to calibrate the instrument response to SSC.
174 Water samples were filtered using pre-weighed 0.4- μ m nitrocellulose filters and washed
175 with freshwater to remove salts. The filters were then dried overnight and re-weighed to
176 determine the volume-concentration of sediment. The OBS measurements were calibrated
177 by comparing the voltage response observed in the field with the measured concentrations
178 from the same time and location, in a method modified from Ogston and Sternberg (1999).
179 Correlation between filtered samples and instrument voltage was strong, with an average
180 r-squared value of 0.83 ± 0.1 . While the sediment concentrations recorded by this near-bed
181 instrument are not directly comparable to the depth-averaged measurements made during
182 the present cross-channel surveys, we herein use these data to extend our understanding
183 of system behavior between the dry and monsoon seasons. For broader context, data from

184 the sensors deployed at the Sutarkhali station are also compared to monthly averaged
185 water discharge for the Ganges and Brahmaputra rivers for the period 1980-2000, based
186 on data from the Bangladesh Water Development Board, and Ganges River sediment
187 discharge data digitized from Lupker et al. (2011).
188

189 To quantify water and sediment flux in this area of the tidal transport system, cross-
190 channel hydrodynamic surveys were conducted during spring and neap tidal conditions at
191 two transects on the Shibsa River during the dry (March 2015) and wet
192 (August/September 2015) seasons. An additional wet season transect was also conducted
193 during moderate tides on the Pussur River. On the Shibsa River, the southern transect was
194 located south of the poldered landscape and entirely within the confines of the Sundarbans
195 forest (Fig.1). The northern transect was located ~12 km upstream in the poldered region,
196 just south of the Dhaki-Shibsa confluence and adjacent to Polder 32 to the east and Polder
197 10-12 to the west (Fig. 1B). Two secondary channels are present between these transect
198 locations that divert water onto the Sundarbans tidal platform and associated creek
199 network. Dry season surveys at both the southern and northern transects took place during
200 peak neap (15-16 Mar) and spring (21-22 Mar) tides. During the ensuing monsoon season,
201 spring tides were measured on August 30-31 (southern transect) and September 2
202 (northern transect), followed by neap tides on September 7 and 8 (northern and southern
203 transects, respectively). Surveys lasted for 11-13 hours as conditions allowed,
204 encompassing approximately one-half of a tidal cycle (i.e., one high and one low tide).
205 Because this system is largely semi-diurnal with a minimal mixed component, we are
206 confident that this time interval was long enough to accurately describe the system
207 dynamics.
208

209 The surveys were conducted using Sontek M9 multi-frequency ADCPs to collect flow-
210 perpendicular observations of current velocity and direction. Data were collected at 1 Hz,
211 using both 1.0 and 3.0 MHz transducers, resulting in vertical bins ranging in height from
212 0.1-1.0 m. From these values, total discharge was calculated by integrating velocity over
213 space and time. River conventions are used for presenting velocity and discharge data,
214 where positive values refer to the ebb or downstream direction and negative values for the
215 flood or upstream transport. A typical survey day included 50-60 individual river crossings
216 at the transect location, measuring cumulative discharge in both directions across the
217 channel. Examples of cross-channel transects of velocity and SSC used to compute
218 instantaneous water and sediment discharge can be found in Figure 2. Because surveys
219 could only be conducted during daylight hours and as weather conditions allowed,
220 discharge is interpolated to complete a 12.4-hour tidal cycle, which is the average tidal
221 cycle duration in the area (range: 11.9-13.1 h). By assuming that the change in tidal prism
222 is negligible between consecutive tides, as suggested by the similarity in tidal elevations
223 (Fig. 3), we can tile measurements in 12.4 h increments and interpolate using a cubic
224 spline. Working conditions were particularly challenging during the monsoon season,
225 resulting in especially short-duration survey days. In the absence of measured discharge,
226 we use a mass balance approach to constrain the magnitude of the missing tidal prism data.
227 For the monsoon-season spring tides, we treat the region between the southern and
228 northern transects and the southern Bhadra River as a closed system with no long-term
229 (>1 semidiurnal period) water storage. Using measured Bhadra River discharge values and

230 assuming a negligible to slightly southerly-directed net flux through the adjacent
231 Sundarbans, allows us to determine the likely range of values for the unmeasured ebb
232 prism at the southern transect. For the monsoon-season neap tides, we consider the larger
233 region bounded by the southern transect to the southwest, the Pussur River below the
234 Dhaki River confluence to the southwest, and the Bangladesh Water Development Board
235 gauging station at the Gorai Railway Bridge ~275 river km to the north. Balancing the
236 measured net flux through the Pussur River and the recorded upstream discharge of the
237 Gorai River of 3000 m³/s with the measured ebb prism at the southern transect allows us
238 to estimate the missing southern transect flood prism. We then repeated this spring tide
239 procedure to estimate the unmeasured neap flood prism at the northern transect.

240

241 **3.3 – Sediment Observations**

242

243 In addition to water discharge, observations of SSC along the transect lines were made
244 using a combination of filtered water samples and optical-backscatter (OBS)
245 measurements. While the exact sampling method varied depending on available
246 instrumentation and river conditions, the general approach involved collecting OBS
247 profiles to the maximum possible depth (<10 m), at either two (northern transect) or three
248 (southern transect) locations along the channel edges and centerline (Figs 1, 2). OBS
249 measurements were supplemented by simultaneous water samples (100-200 ml) collected
250 from various depths using a Niskin sampler, which were used to calibrate the OBS as
251 described above (Section 3.1).

252

253 In order to calculate total sediment fluxes, the vertically and horizontally distributed SSC
254 observations collected for each channel cross-section were averaged to produce a series of
255 temporally discrete SSC values over the course of one tidal cycle (Figs 2, 4). This spatial
256 averaging appears suitable because the variance was considerably smaller than the
257 temporal variability associated with tidal discharge and strong seasonal contrasts. Using
258 wet season data as an example, the average standard deviation of SSC through time at one
259 sample location was 0.2 g/L, while the average standard deviation of SSC between stations
260 at any given time was 0.13 g/L. When conditions did not allow samples to be collected at
261 depths below the water surface, a scaling factor of 1.25 was applied to account for the
262 higher sub-surface SSC, which we determined by the relationship between depth-averaged
263 concentrations and surface concentrations from the other available data. Similarly,
264 measurements from 15 March (dry-season neap tide) were only collected at depths of 5
265 and 15 m and were thus scaled by a factor of 0.81 to be comparable to other measurements
266 that included surface SSC values.

267

268 An important caveat for all SSC measurements is that we present data collected primarily
269 from the upper water column and not sampled isokinetically, due to instrument limitations
270 and high current velocities. Thus, our values principally represent suspended load and do
271 not account for bedload transport, which likely represents an additional component of total
272 sediment transport. As with our water-discharge measurements, SSC values were
273 calculated over an entire tidal cycle by repeating a measured time series in 12.4-hour
274 increments, then interpolating using a cubic spline. From these values, the integrated

275 product of water discharge and SSC yields net sediment flux, which we compute using the
276 time series for each component as calculated using the aforementioned methods.

277

278

279 **4 – Results**

280

281 **4.1 – Long-term Pressure and OBS**

282

283 At our long-term station deployed in a secondary tidal channel (Fig. 1), recorded water-
284 level variations show tidal-period excursions with a range of 1.8 to 4.8 m over the 12
285 months of observation (Fig. 3). This variance is, of course, driven primarily by the
286 fortnightly spring-neap tidal cycle, but there is also a seasonal variability showing the
287 monsoon period to have a reduced tidal range as compared with the dry season. In this
288 case, the neap tidal range is ~10% less during the monsoon season, and the spring tidal
289 range is as much ~20% less, accounting for a nearly 1 m difference (3.9 m vs. 4.8 m). This
290 reduced range in the monsoon season, however, is not manifested in the elevation of high-
291 tide water levels, which remained largely consistent between seasons. Rather, the
292 difference is caused by higher water levels during low tide (Fig. 3), which has the effect of
293 truncating the tidal range and yielding an overall higher mean water level. These higher
294 low-water levels associated with the monsoon suggest that they are tied to regional
295 freshwater drainage and discharge. In addition, another contributing factor could be the
296 seasonally reversing monsoon wind stresses, but such set-up should enhance high water
297 levels as well, suggesting that they are not the primary cause. Although further research on
298 this topic is needed, these distinctions are important herein for understanding the behavior
299 of the tidal delta plain, as landscape elevations in this region are closely tied to mean high-
300 tide water levels, and not mean sea level (Auerbach et al., 2015). Thus, as first
301 demonstrated by Pethick and Orford (2013), the monthly mean tide-gauge data often used
302 to track seasonal to interannual variations in water level may have relatively little bearing
303 on the tidal inundation period and sedimentation rates that control tidal platform elevation
304 (Rogers et al. 2013).

305

306 The arrival of fully fresh water (wet-season) conditions occurs in July, following the peak in
307 Brahmaputra River water discharge, and roughly coincident with peak Ganges River water
308 discharge (Fig. 4). Coupled with our long-term pressure gauge, the OBS sensor recorded
309 relatively constant, but low, mean SSC from the late dry season into the early monsoon
310 period (late March through July), with weak but noticeable spring-neap variability ranging
311 from ~0.01 g/L to 0.20 g/L (Fig. 3). However, moving into peak monsoon season, SSC
312 increases markedly from early August through September, concurrent with the Ganges
313 River sediment discharge peak (Figs 2, 3). Individual measurements regularly exceeded
314 0.50 g/L during this time, with maxima >2.5 g/L (Fig. 3). SSC variability around the semi-
315 diurnal tide and spring-neap cycles was greatly enhanced compared with that during the
316 dry season, with SSC values during spring tidal cycles exceeding those observed during
317 neap conditions by a factor of 2-10. By the end of observations in October 2015, SSC began
318 to drop to levels similar to those observed in mid-August (0.01-1.0 g/L; Fig. 3), but on
319 average remained well above those of the dry season. For comparison, the mean annual
320 SSC of the mainstem Ganges-Brahmaputra river is ~1 g/L, and depth-averaged values in

321 the main estuary mouth and on the inner shelf commonly range 2-5 g/L during high river
322 discharge (Barua et al., 1994; Ali et al., 2013). In total, SSC values well in excess of 1 g/L are
323 regularly observed during the wet season from the mainstem river to the inner shelf and
324 into the tidal channels of the lower delta plain. These results support previous evidence for
325 the strong coupling of seasonal river discharge with penecontemporaneous sedimentation
326 in the remote tidal delta plain (Rogers et al., 2013).

327

328 **4.2 - Hydrography - Water Discharge**

329

330 Dry season tidal range on the Shibsra River, as measured at Nalian near the northern
331 transect (Fig. 1B), varied from 2.3 m during the neap minima to 5.6 m during spring
332 maxima (Fig. 3). The tidal period was slightly longer during neap tides than spring tides
333 (12.9 h vs. 12.3 h), and the mixed component of the semi-diurnal tide was more
334 pronounced, with consecutive tidal ranges varying by as much as 0.55 m during neap tides,
335 versus 0.23 m during spring tides (Fig. 3). During the monsoon fieldwork, the tidal range
336 was 2.4 and 4.2 m for neap and spring tides, respectively. As with the dry season, total tidal
337 period during neap tides was slightly longer than spring tides (12.8 h vs. 12.0 h). The mixed
338 semi-diurnal variability was again greater during neap tides as well, which varied by as
339 much as 0.25 m, while spring tide variability was typically <0.10 m (Fig. 3).

340

341 In this study, we calculate the tidal prism by integrating water discharge over the
342 individual ebb and flood limbs of the tide, with net discharge calculated as the difference
343 between them. During the dry season, our observations captured both peak flood and ebb
344 discharges, with interpolation being used over the remaining <5-15% of the tidal cycle (Fig.
345 5). During the wet season, field conditions during several surveys limited our measurement
346 to only a partial tidal cycle (~8-9 hr survey; Fig. 5). Only during northern transect spring
347 tides were conditions favorable for collecting observations of similar duration to the dry
348 season (~11 hr survey; Fig. 5). Within these limits, however, we have used conservative
349 interpolation methods to generate error-bound estimates of total water discharge, the
350 resulting patterns of which provide robust observations concerning system behavior (see
351 Section 2; Fig. 5).

352

353 The average tidal-prism magnitudes for the northern and southern transects are $2.1 \pm 0.7 \times$
354 10^8 m^3 and $3.4 \pm 1.4 \times 10^8 \text{ m}^3$, respectively. Included in these averages are the absolute
355 values of flood and ebb tidal prisms measured on spring and neap tides during both wet
356 and dry seasons (Table 1). Thus, the tidal prism at the northern transect averages only
357 ~60±10% that of the southern transect regardless of season, even though they are located
358 just 10 km apart. Most of this difference in discharge (c. 80-100%) can be balanced by
359 water storage between the two locations, where the product of tidal range and area
360 between transects is c. $6.7 \times 10^7 \text{ m}^3$. Considering differences in seasonal discharge, results
361 show that the neap ebb prism is ~30% greater during the monsoon at both transects,
362 despite having a smaller tidal range compared with the dry season survey. This difference
363 of $4\text{-}6 \times 10^7 \text{ m}^3$ equates to an excess ebb discharge of 1800-2800 m^3/s , which is about 45-
364 70% of the mean monsoon discharge of the upstream Gorai River. We thus take the greater

365 wet-season ebb prism to simply reflect the addition of local freshwater discharge from the
366 Gorai River (Table 1; Fig. 1).

367
368 Strictly speaking, defining a tidal regime as either ebb- or flood- dominant refers to the
369 water velocity rather than discharge (Pethick, 1980; Brown and Davies, 2010). In the
370 present study, however, we are interested in the net movement of water and sediment and
371 thus refer to a particular discharge regime as either ebb or flood “dominated” or “oriented”
372 based on the net tidal prism (i.e., the difference between ebb and flood discharge). With
373 this in mind, our surveys suggest that the system varies between ebb and flood orientation
374 across both tidal phase and season (Table 1). For example, both transects during the dry,
375 spring and wet, neap surveys show the average ebb-tidal prism to be $26\pm 16\%$ larger than
376 the flood limb. In contrast, the other two survey periods (dry, neap and wet, spring)
377 yielded balanced to slightly flood dominated tidal prisms ($9\pm 8\%$). In summary, although
378 our results on water balance are insufficient for a full understanding of the patterns, a key
379 finding is that the ebb and flood tidal prisms rarely balance at this location. These tidal-
380 prism asymmetries appear to be a salient characteristic of the complex, interconnected
381 channel network of the GBMD tidal delta plain. Thus, even our limited observations require
382 a lateral (east-west) exchange of water between the Shibsra and parallel Pussur channels
383 (Fig. 1), which we presume to be driven by locally non-uniform tidal phasing within the
384 channel network. Given these emergent circulation patterns, it is clear that individual
385 channels do not operate as closed systems and exhibit local, non-uniform mass exchange,
386 providing a first indication of how morphologic evolution of this tidal delta plain and its
387 channel network may occur.

388
389 Although relative dominance between the ebb and flood tidal prisms persistently covaries
390 (as described above), the mean and instantaneous water discharge (m^3/s) is almost always
391 flood-dominant (Fig. 6). This circumstance arises from the significant phase shift that
392 occurs as the tide wave propagates up channel, resulting in a shorter flood period and thus
393 higher peak discharge. From our measurements of instantaneous discharge across seasons
394 and tidal conditions, we calculate mean ebb and flood discharges (m^3/s) for each transect
395 (Fig. 6). Mean discharge for the northern transect is $\sim 9100 \text{ m}^3/\text{s}$ on the flood and 8600
396 m^3/s on the ebb, and for the southern transect, mean flood and ebb discharges are $\sim 14,600$
397 and $14,200 \text{ m}^3/\text{s}$, respectively. From these results, we observe that mean discharge at the
398 northern transect is again $\sim 61\pm 1\%$ that of the southern transect, as also recognized for the
399 tidal prism. Another notable result is that the mean flood discharge (m^3/s) is 3-6% greater
400 than on the ebb tide, despite the tidal prism generally being ebb dominant. This disparity is
401 a function of the shallow-water distortion of the M2 tide, which produces an asymmetrical
402 waveform with a steeper rising limb than falling limb, and a corresponding reduction in the
403 duration of the flood tide by $\sim 60\text{-}90$ minutes.

404
405

406 **4.3 – Hydrography – Sediment Transport**

407
408 Suspended sediment measurements collected during the hydrographic surveys show
409 similar patterns to those of our long-term OBS station. Wet season sediment concentrations
410 were generally 30-50% higher than during the dry season (Fig. 5). Much greater

411 differences in SSC were observed, however, between neap and spring tidal conditions, with
412 the latter concentrations being typically ~3 fold greater (0.3-1.5 g/L vs 0.1-0.5 g/L). These
413 sediment concentrations, coupled with the water discharge observations, were then
414 extrapolated over the tidal cycle to generate estimates of the rates and magnitude of
415 sediment transport (Table 1). Results show that integrated sediment transport over a tidal
416 limb varied by more than an order of magnitude at both transects. Minima of 0.16×10^8 kg
417 (north) and 0.2×10^8 kg (south) of sediment exchange were observed during the neap, dry-
418 season ebb tide, with maxima during spring, monsoon flood tides being an order of
419 magnitude greater at 3.3×10^8 kg (north) and 3.9×10^8 kg (south) . These values equate to
420 mean rates of sediment transport ranging from ~700 kg/s during neap, dry season
421 conditions to ~17,000 kg/s during monsoon-season spring tides. Comparing the ebb and
422 flood limbs of our surveys, the mean sediment discharge for the ebb tide is 5800 kg/s
423 compared to 7800 kg/s for the flood tide, demonstrating an overall flood dominance in
424 sediment transport.

425
426 These patterns are further supported by the net sediment transport values (i.e., ebb – flood;
427 Table 1). For a given tidal cycle, net sediment transport was typically 10^6 - 10^7 kg, with
428 magnitude varying largely with tidal phase, where spring tides generate 1.5 to 3 times
429 greater net transport than during neap tides (Table 1). Seasonally, net sediment transport
430 rates were ~30% greater during the wet season, similar to our observations of suspended
431 sediment concentration. Finally, a comparison of net sediment transport with
432 corresponding net water discharge shows the two to covary, as expected, with greater net
433 water discharge resulting in greater net sediment transport (Fig. 7). However, an important
434 attribute of this relationship reveals a significant bias toward flood-dominant sediment
435 transport. Data show that even neutral to weakly ebb dominant water discharge yields net
436 sediment transport in the flood direction (Fig. 7). As noted for water discharge (m^3/s), this
437 disparity is a function of the non-negligible tidal components beyond M2 that result in a
438 shortened flood limb and extended ebb period (Fig. 3; Table 1). Together, mean sediment
439 discharge and net sediment transport patterns thus indicate an overall flood-oriented
440 asymmetry and net onshore transport of sediment.

441

442

443 **5 - Discussion**

444

445 **5.1 - Relative importance of tides and river**

446

447 The GBM tidal delta plain comprises a complex channel network that has been little studied
448 and will require substantial investigation to be understood well. Nevertheless, results of
449 the current study allow for numerous observations on the scaling and magnitude of tidal
450 mass transport within this region, establishing a baseline for the role that tides play in
451 defining the delta system, particularly in the southwest region away from direct fluvial
452 inputs. To begin, we take an average of the flood and ebb tidal prisms measured at the two
453 sites on the Shibsra River over both spring and neap tidal phases during wet and dry
454 seasons, and extrapolate the mean tidal prism over one year. In other words, an average of
455 2.7×10^8 m^3 water passes through this region on each of the ~705 tides per year. This basic

456 estimation accounts for an average of $\sim 2 \times 10^{11} \text{ m}^3$ of water annually conveyed through
457 our survey locations, 80 km inland of the coast. Furthermore, this mass exchange is
458 principally tidal water, as the 50-75% of annual Gorai River discharge captured by the
459 Shibsra River (i.e., $\sim 0.2 \times 10^{11} \text{ m}^3$) accounts for only 10% of the total water exchange
460 observed for that channel.

461
462 The significance of these observations from the upstream Shibsra River tidal channel
463 become more apparent when compared with the mainstem GBM rivers. In this case, the ~ 2
464 $\times 10^{11} \text{ m}^3$ of water conveyed annually through the upper Shibsra River is nearly 20% of the
465 $\sim 11 \times 10^{11} \text{ m}^3$ of total annual water discharge from the entire GBM watershed (Lupker et
466 al., 2011; Fig. 4). This is an impressive exchange of mass through the upper reaches of a
467 single tidal channel along the GBM tidal delta plain. For context, the Shibsra River
468 comprises approximately half (by planform area) of the Pussur River tidal system (Fig. 1),
469 itself just one of five major tidal drainages along the GBM tidal delta plain (Fig. 1). Taken
470 together, these basins include ~ 10 tidal channels having similar area (width \times length) to
471 the Shibsra River. We take the tidal flow through these systems to be broadly similar given
472 the linear relationship between peak tidal discharge and the cross-sectional area of large
473 tidal channels (Rinaldo et al., 1999), plus the fact that land-surface elevation and tidal range
474 are similar across the region (Chatterjee et al., 2013). Thus, even at a first-order, estimates
475 of total mass transport across the tidal region would well exceed the $\sim 11 \times 10^{11} \text{ m}^3$ total
476 volume discharged by the mainstem GBM rivers.

477
478 The comparable values between our observations of tidal water exchange in this limited
479 study area and the total freshwater discharge of the GBM rivers demonstrates how tides
480 hold equivalence in controlling landscape development in the GBMD, which was suggested
481 as far back as Galloway (1975). To further consider the geomorphic importance of tides to
482 the GBMD, we make analogous estimations of the sediment transport (Q_s) that supports
483 land-surface aggradation and the dominant water discharge (Q_{dom}) that controls tidal
484 channel morphology (Rinaldo et al., 1999). As done for water discharge, by taking the
485 average of our tidal hydrography data for sediment transport, we calculate a mean annual
486 exchange of suspended sediment through the Shibsra River tidal station to be $\sim 1 \times 10^{11} \text{ kg}$
487 ($\sim 100 \text{ Mt}$). For comparison, this estimate of sediment load is roughly 15% of the $\sim 700 \text{ Mt}$
488 of sediment annually discharged to the coast by the GBM rivers (Goodbred and Kuehl,
489 1999). Thus, if we extrapolate any similar transport value to the other nine GBM tidal
490 channels, then the sediment exchange through the tidal channels is easily found to be
491 comparable to the main river mouth. There is, of course, the important caveat that tidal
492 sediment transport is not unidirectional, and so this integrated exchange of tidal sediment
493 is not a net flux as it is for river sediment discharge. Nevertheless, the relevant point is that
494 local, geomorphic reaches of the tidal delta plain have the opportunity for landscape
495 building through tidal water and sediment exchange at a similar magnitude to the
496 mainstem GBM rivers. This assertion is not surprising given the relative stability of the
497 tidal delta plain, which experiences relatively little net erosion ($\sim 4 \text{ km}^2/\text{yr}$, or $\sim 0.02\%$
498 annual loss; Sarwar and Woodroffe, 2013) and is offset by widespread sediment deposition
499 on both land-surface (Rogers et al., 2013) and in channels (Wilson et al., 2017).

500

501 From this study, we understand that tidal energy, independent of the main river mouth,
502 accounts for a twice-daily exchange of a mass equivalent to 4-15% of the yearly averaged
503 daily GBM river discharge. In primary channels, the magnitude of this exchange is
504 controlled more by the spring-neap tidal variability than by the seasonal input of new
505 material (Fig. 5). In the smaller Bhadra tidal channel, on the other hand, SSC variability
506 demonstrates profound seasonality, presumably because discharge (and therefore stream
507 power) is at least an order of magnitude smaller here than in the Shibsra River. This
508 disparity is important when we consider land-building processes, as the majority of the
509 Sundarbans forest is plumbed by tidal channels on the scale of the Bhadra River or smaller.
510 Storms may also play a role in remobilizing sediment from the shelf onto the tidal
511 delpalain, as suggested by Hanebuth et al. (2013) in their study of ancient salt kilns buried
512 along the coast. However, there are no observations of significant direct storm deposition
513 from recent cyclones (Aila, 2009 and Sidr, 2007), such as that recognized from the offshore
514 Bengal shelf and Swatch-of-No-Ground canyon (e.g., Kudrass et al., 1998; 2018; Michels et
515 al., 1998; Rogers et al., 2015). The potentially limited impact of storms on sedimentation
516 and the channel network of the tidal delpalain may be due its frequent and persistent
517 exposure to high sediment concentrations and strong currents (>3 m/s) driven by the
518 tides. Nevertheless, future research should aim to quantify storm inputs and their relative
519 importance upon sedimentation and morphodynamics of the tidal delpalain.

520
521 These findings and discussion points emphasize the essential role that tides play in
522 maintaining the largest portion of the GBM lower delta plain, which is not under direct
523 river influence. However, despite the essential role of tides in mixing and dispersing
524 sediment to large areas of the delta, the supply of sediment remains largely
525 contemporaneous with seasonal fluvial discharge, especially in the secondary and tertiary
526 channels that irrigate the Sundarbans. Together, the coupled system in which the GBM
527 rivers deliver sediment that is subsequently redistributed by tidal energy is fundamentally
528 responsible for sustainability of this region relative to sea-level change (e.g., Angamuthu et
529 al., 2018). A significant corollary of this fact is that a change in sediment supply from the
530 GBM rivers, such as that proposed under India's National River Linking Project, could pose
531 a serious threat to delta sustainability (Higgins et al., 2018; Best, 2019).

532
533 To summarize, as the central coastal region receives little direct water and sediment
534 discharge from the GBM, the results herein emphasize that tidal exchange is the dominant
535 geomorphic agent in the region with a mass and energy exchange of comparable or greater
536 magnitude to the mainstem rivers. It is, of course, essential to recognize that most
537 freshwater and sediment exchanged within the tidal system is ultimately sourced by the
538 main rivers, and that these are intrinsically coupled systems. Thus, continued sustainability
539 of the region will require the sustained delivery and exchange of water and sediment
540 between the fluvial and tidal portions of the delta.

541 542 **5.2 – Sedimentation in the Sundarbans and Infilling of Tidal Channels**

543
544 Our observations of tidal sediment exchange provide a useful baseline for examining
545 sedimentation in the Sundarbans and broader tidal delta plain, which are at risk from sea-
546 level rise and inundation without an adequate supply of sediment. To date, the best

547 estimate of total sedimentation in the Sundarbans is 1.1×10^{11} kg/year (~ 100 Mt), based
548 on one season of direct sedimentation measures at 48 stations across the region (Rogers et
549 al., 2013). This mass of sediment deposited in the Sundarbans is basically equivalent to the
550 ~ 100 Mt of sediment that we observe transported through the Shibs River transects.
551 Thus, recalling that our local measurements likely capture just 5-10% of total suspended
552 sediment transported through the tidal channels of the region, it becomes evident that
553 there is generally adequate suspended sediment available to support regional
554 sedimentation in the Sundarbans.

555
556 Another plausible implication is that there appears to be adequate sediment available for
557 the restoration of land elevation within the poldered region, which is a major challenge
558 facing coastal Bangladesh (Amir et al., 2013). Although a definitive answer remains to be
559 determined, this general assertion is supported by observations of the rapid sedimentation
560 that occurred on Polder 32 in the two years following the embankment failures caused by
561 cyclone Aila in 2009 (Auerbach et al., 2015). Measurements at Polder 32 after these
562 failures found an average of 37 ± 17 cm/yr of tidal sedimentation sustained over its two-
563 year exposure to tidal inundation, corresponding to a total annual deposition of ~ 5 Mt.
564 Based on inundation depth and period, this accounts for an average of ~ 0.2 g/L of sediment
565 extracted from the tidal waters that flooded the island during this time. This value
566 compares to a mean suspended sediment concentration of ~ 0.6 g/L measured during our
567 hydrographic surveys, suggesting that roughly one-third of the tidal sediment inundating
568 the landscape generated these very rapid sedimentation rates. Ultimately, limitations in the
569 present data preclude a closed, precise sediment budget, but our collective observations
570 over several different studies remain consistent in direction and magnitude. These indicate
571 persistent, relatively rapid, rates of deposition that are sustained by the large-magnitude
572 conveyance of sediment through the tidal channels and ultimately supplied by seasonal
573 discharge of the mainstem rivers (Rogers et al., 2013; Auerbach et al., 2015; this study).

574
575 Upstream of our transect sites, the landscape is almost entirely embanked by polder
576 systems. With limited opportunity for sediment deposition on this formerly intertidal
577 platform, and with the resulting reduction or redistribution of the tidal prism upstream,
578 channel sedimentation and infilling has become a major problem. Wilson et al. (2017)
579 demonstrate that by preventing the inundation of the intertidal platform, poldering has
580 reduced the tidal prism of the broader southwest region by as much as 1.4×10^9 m³. If we
581 assume that this volume reduction is relatively evenly dispersed across the delta plain,
582 then it would have led to a 25-50% reduction in the local tidal prism measured at our sites.
583 These effects are at least partially responsible for the ~ 1400 km of channel infilling that
584 has taken place over the last few decades, resulting in the creation of new agriculture and
585 aquaculture opportunities but also altering drainage, transportation routes, and feedback
586 responses of the regional tidal hydrodynamics (Wilson et al., 2017). The mass of sediment
587 that has infilled these channels is calculated to be 6.15×10^{11} kg, which would be $\sim 1.2 \times$
588 10^{10} kg/yr assuming a roughly constant rate (Wilson et al., 2017). Of these infilled
589 channels, $\sim 15\%$ (~ 200 km) are part of the former channel network connecting upstream
590 of our northern transect (Fig. 1). Thus, a proportional rate of sedimentation lost to these
591 channels would be $\sim 0.18 \times 10^{10}$ kg/yr, which is $\sim 25\%$ of the estimated 0.68×10^{10} kg

592 fluxing through the northern transect (to the north) each year. While this sediment
593 exchange is four times greater than the expected total based on infilling rates from Wilson
594 et al. (2017), it relies on the same previously described assumptions (i.e., no lateral
595 exchange with neighboring rivers, non-end-member flux reflecting an average of end-
596 member conditions). More importantly, it appears that there is sufficient sediment
597 available to continue infilling channels, and future studies should constrain whether this
598 region is, in fact, infilling faster than other areas on the tidal delta plain, as this would hold
599 important implications for regional navigation and hydrodynamic changes.

600

601 **6 - Conclusions**

602

603 In the present study, we have measured tidal and seasonal variability associated with
604 water discharge and suspended sediment concentration (SSC), and used these observations
605 to compute the magnitude of water and sediment exchange through a single tidal channel.
606 As has been suggested previously, the wet season is found to exert a strong control on the
607 timing and magnitude of sediment transport in this system, despite seemingly modest
608 changes to the hydrodynamics. Indeed, despite a reduced tidal range and similar peak SSC,
609 sediment transport during the monsoon is always of greater magnitude than during the dry
610 season. Understanding this relationship is critical for planning any potential land recovery
611 strategies in the future. The importance of the monsoon also provides a new perspective
612 into the meaning of a “tidal delta.” While it is clearly the tides that perform much of the
613 work to shape the delta – including driving a net flood-oriented direction of sediment flux –
614 it is the seasonal influx of riverine sediment that allows this work to continue. Finally, this
615 research demonstrates that the mass of sediment transported north of our study area is
616 more than sufficient to fill channels and create additional land. Ideally, future land-use
617 management strategies could divert some of this excess sediment into polder interiors
618 through tidal river management (e.g., Seijger et al., 2018; Shampa et al., 2012; van Staveren
619 et al., 2016), and allow this landscape to continue to prosper.

620

621 **Code availability:**

622

623 **Data availability:**

624 Data used for this publication will be archived in the Marine Geoscience Data System.

625

626 **Sample availability:**

627 Samples from this publication are stored in the sedimentology laboratory at Vanderbilt
628 University

629

630 **Author Contribution:**

631 The experiment was designed by RH and SG, with input from RB and JB. RH and RB led the
632 field research efforts with support from SG and JB. RH wrote the majority of the manuscript
633 and figures, with substantial input from SG. RB and JB also contributed to the manuscript
634 and figures.

635

636 **Competing interests:**

637 The authors declare that they have no conflict of interest.

638
639
640
641
642
643
644
645
646
647
648
649
650
651
652

Acknowledgements:

This work would not be possible without the support of our local collaborators, Drs Kazi Matin Ahmed and Syed Humayun Akchter from Dhaka University, who oversaw in-country logistics and offer local guidance. We would also like to thank Abu Naser Hossain of the Forestry Crime Department for his help with permitting, and Nasrul Islam Bachchu of Pugmark Tours, and the captain and crew of the M/V Bawali and M/L Mawali for their seemingly endless patience with our field logistics. We would also like to thank Md. Saddam Hossain, Abrar Hossain, Mynul Hassan, Carol Wilson, and Mike Reed for their field support. This research was supported by the US Office of Naval Research (N00014-11-1-0683) and the National Science Foundation (Coastal SEES- #1600319).

653 **References:**

- 654
- 655 Alam, M.A., Hossain, M.A., and Shafee S. Frequency of Bay of Bengal cyclonic storms and
656 depressions crossing different coastal zones. *International Journal of Climatology*, 23,
657 pp. 1119-1125, 2003.
- 658 Ali, A., Mynett, A.E. and Azam, M.H. Sediment dynamics in the Meghna estuary, Bangladesh:
659 A model study. *Journal of Waterway Port Coastal and Ocean Engineering-ASCE*, 133:
660 255-263, 2007.
- 661 Allison, M. and Kepple, E. Modern sediment supply to the lower delta plain of the Ganges-
662 Brahmaputra River in Bangladesh. *Geo-Marine Letters*, 21(2), pp.66-74, 2001.
- 663 Alongi, D.M. Carbon cycling and storage in mangrove forests. *Annual Review of Marine*
664 *Science*, 6, pp.195-219, 2014.
- 665 Amir, M.S.I.I., Khan, M.S.A., Khan, M.K., Rasul, M.G. and Akram, F. Tidal river sediment
666 management-A case study in southwestern Bangladesh. *International Journal of*
667 *Environmental, Chemical, Ecological, Geological and Geophysical Engineering*, 7(3),
668 pp.176-185, 2013.
- 669 Angamuthu, B., Darby, S.E., and Nicholls, R.J. Impacts of natural and human drivers on the
670 multi-decadal morphological evolution of tidally-influenced deltas. *Proceedings of the*
671 *Royal Society A*, 474, 20180396, 2018.
- 672 Anthony, E.J., Brunier, G., Besset, M., Goichot, M., Dussouillez, P. and Nguyen, V.L. Linking
673 rapid erosion of the Mekong River delta to human activities. *Scientific Reports*, 5,
674 p.14745, 2015.
- 675 Auerbach, L.W., Goodbred Jr, S.L., Mondal, D.R., Wilson, C.A., Ahmed, K.R., Roy, K., Steckler,
676 M.S., Small, C., Gilligan, J.M. and Ackerly, B.A. Flood risk of natural and embanked
677 landscapes on the Ganges–Brahmaputra tidal delta plain. *Nature Climate Change*, 5(2),
678 p.153, 2015.
- 679 Ayers, J. C., George, G., Fry, D., Benneyworth, L., Wilson, C., Auerbach, L., Roy, K., Karim, M.R.,
680 Akter, F., Goodbred, S. Salinization and arsenic contamination of surface water in
681 southwest Bangladesh. *Geochemical Transactions*, 18(1), 4, 2017.
- 682 Barua, D. K., Kuehl, S. A., Miller, R. L., & Moore, W. S. Suspended sediment distribution and
683 residual transport in the coastal ocean off the Ganges-Brahmaputra river
684 mouth. *Marine Geology*, 120(1-2), 41-61, 1994.
- 685 Best, J. Anthropogenic stresses on the world’s big rivers. *Nature Geoscience*, 12, pp 7-21,
686 doi: <https://doi.org/10.1038/s41561-018-0262-x>, 2019.
- 687 Brammer, H. Bangladesh’s dynamic coastal regions and sea-level rise. *Climate Risk*
688 *Management*, 1, pp.51-62, 2014.
- 689 Brown, J.M. and Davies, A.G. Flood/ebb tidal asymmetry in a shallow sandy estuary and the
690 impact on net sand transport. *Geomorphology*, 114(3), pp.431-439, 2010.
- 691 Brown, S. and Nicholls, R.J. Subsidence and human influences in mega deltas: the case of the
692 Ganges–Brahmaputra–Meghna. *Science of the Total Environment*, 527, pp.362-374,
693 2015.
- 694 Chatterjee, M., Shankar, D., Sen, G.K., Sanyal, P., Sundar, D., Michael, G.S., Chatterjee, A.,
695 Amol, P., Mukherjee, D., Suprit, K. and Mukherjee, A. Tidal variations in the Sundarbans
696 estuarine system, India. *Journal of Earth System Science*, 122(4), pp.899-933, 2013.

697 Darby, S.E., Hackney, C.R., Leyland, J., Kummu, M., Lauri, H. Parsons, D.R., Best, J.L, Nicholas,
698 A.P. and Aalto, R. Fluvial sediment supply to a mega-delta reduced by shifting tropical-
699 cyclone activity. *Nature*, 539, 276-279, doi:10.1038/nature19809, 2016.

700 Darby, S.E., Nicholls, R.J., Rahman, M.M., Brown, S. and Karim, R. A Sustainable Future
701 Supply of Fluvial Sediment for the Ganges-Brahmaputra Delta. In *Ecosystem Services for*
702 *Well-Being in Deltas* (pp. 277-291). Palgrave Macmillan, Cham, 2018.

703 Ericson, J.P., Vörösmarty, C.J., Dingman, S.L., Ward, L.G. and Meybeck, M. Effective sea-level
704 rise and deltas: causes of change and human dimension implications. *Global and*
705 *Planetary Change*, 50(1-2), pp.63-82, 2006.

706 Galloway, W.E. Process framework for describing the morphologic and stratigraphic
707 evolution of deltaic depositional systems in M.L. Broussard, ed. *Deltas: models for*
708 *exploration*, pp. 87-98, Houston Geological Society, 1975.

709 Goodbred Jr, S.L. and Kuehl, S.A. Holocene and modern sediment budgets for the Ganges-
710 Brahmaputra river system: Evidence for highstand dispersal to flood-plain, shelf, and
711 deep-sea depocenters. *Geology*, 27(6), pp. 559-562, 1999.

712 Grinsted, A. Tidal fitting toolbox (v 1.3.0.0), Matlab code,
713 [https://www.mathworks.com/matlabcentral/fileexchange/19099-tidal-fitting-](https://www.mathworks.com/matlabcentral/fileexchange/19099-tidal-fitting-toolbox?s_tid=srchtitle)
714 [toolbox?s_tid=srchtitle](https://www.mathworks.com/matlabcentral/fileexchange/19099-tidal-fitting-toolbox?s_tid=srchtitle), 2008.

715 Hanebuth, T.J.J., Kudrass, H.R., Linstadter, J., Islam, B., and Zander, A.M. Rapid coastal
716 subsidence in the central Ganges-Brahmaputra Delta (Bangladesh) since the 17th
717 century deduced from submerged salt-producing kilns. *Geology*, 41(9), pp.987-990,
718 2013.

719 Higgins, S.A., Overeem, I., Steckler, M.S., Syvitski, J.P., Seeber, L. and Akhter, S.H. InSAR
720 measurements of compaction and subsidence in the Ganges-Brahmaputra Delta,
721 Bangladesh. *Journal of Geophysical Research: Earth Surface*, 119(8), pp.1768-1781,
722 2014.

723 Higgins, S., Overeem, I., Rogers, K. and Kalina, E. River linking in India: Downstream impacts
724 on water discharge and suspended sediment transport to deltas. *Elem Sci Anth*, 6(1),
725 2018.

726 Hossain, M.S., Dearing, J.A., Rahman, M.M, and Salehin, M. Recent changes in ecosystem
727 services and human well-being in the Bangladesh coastal zone. *Regional*
728 *Environmental Change* 16(2):429-443, 2016.

729 Islam, M.R. Managing Diverse Land Uses in Coastal Bangladesh: Institutional
730 Approaches. *Environment and livelihoods in tropical coastal zones*, p.237, 2006.

731 Kamal, A.S.M., Hossain, A., Hossain, B.M., Hassan, S.M. and Rashid, A.K.M. Physical and Social
732 Assessment of the Waterlogged Area and Suitability of the “Inclusive and Adaptive
733 Tidal River Management Technique” to Alleviate Waterlogging in Southwest
734 Bangladesh. *Procedia Engineering*, 212, pp.760-767. , 2018.

735 Khadim, F.K., Kar, K.K., Halder, P.K., Rahman, M.A. and Morshed, A.M. Integrated water
736 resources management (IWRM) impacts in south west coastal zone of Bangladesh and fact-
737 finding on tidal river management (TRM). *Journal of Water Resource and*
738 *Protection*, 5(10), p.953, 2013.

739 Kudrass H.R., Michels K.H., Wiedicke M., Suckow A. Cyclones and tides as feeders of a
740 submarine canyon off Bangladesh. *Geology*, 26, pp.715-718, 1998.

741 Kudrass, H.R., Machalett, B., Palamenghi, L., Meyer, I., and Zhang, W. Sediment transport by
742 tropical cyclones recorded in a submarine canyon off Bangladesh. *Geo-Marine Letters*,
743 38(6), pp.481-496.

744 Lupker, M., France-Lanord, C., Lavé, J., Bouchez, J., Galy, V., Métivier, F., Gaillardet, J.,
745 Lartiges, B., and Mugnier, J.L. A Rouse-based method to integrate the chemical
746 composition of river sediments: Application to the Ganga basin. *Journal of Geophysical*
747 *Research: Earth Surface*, 116, pp.1–24, 2011.

748 Marois, D.E. and Mitsch, W.J. Coastal protection from tsunamis and cyclones provided by
749 mangrove wetlands—a review. *International Journal of Biodiversity Science, Ecosystem*
750 *Services & Management*, 11(1), pp.71-83, 2015.

751 Mcleod, E., Chmura, G.L., Bouillon, S., Salm, R., Björk, M., Duarte, C.M., Lovelock, C.E.,
752 Schlesinger, W.H. and Silliman, B.R. A blueprint for blue carbon: toward an improved
753 understanding of the role of vegetated coastal habitats in sequestering CO₂. *Frontiers*
754 *in Ecology and the Environment*, 9(10), pp.552-560, 2011.

755 Michels, K.H., Kudrass, H.R., and Hu, C. The submarine delta of the Ganges- Brahmaputra :
756 cyclone-dominated sedimentation patterns. *Marine Geology*, 149, pp.133–154, 1998.

757 Nowreen, S., Jalal, M.R. and Khan, M.S.A. Historical analysis of rationalizing South West
758 coastal polders of Bangladesh. *Water Policy*, 16(2), pp.264-279, 2014.

759 Ogston, A.S. and Sternberg, R.W. Sediment-transport events on the northern California
760 continental shelf. *Marine Geology*, 154(1-4), pp.69-82, 1999.

761 Overeem I. and Syvitski, J.P.M. Dynamics and Vulnerability of Delta Systems: LOICZ Reports
762 and Studies, No 35, GKSS Research Center, Geesthacht, 54 p., 2009.

763 Pendleton, L., Donato, D.C., Murray, B.C., Crooks, S., Jenkins, W.A., Sifleet, S., Craft, C.,
764 Fourqurean, J.W., Kauffman, J.B., Marbà, N. and Megonigal, P. Estimating global “blue
765 carbon” emissions from conversion and degradation of vegetated coastal
766 ecosystems. *PloS One*, 7(9), p.e43542, 2012.

767 Pethick, J.S. Velocity surges and asymmetry in tidal channels. *Estuarine and Coastal Marine*
768 *Science*, 11(3), pp.331-345, 1980.

769 Pethick, J. and Orford, J.D. Rapid rise in effective sea-level in southwest Bangladesh: its
770 causes and contemporary rates. *Global and Planetary Change*, 111, pp.237-245, 2013.

771 Rinaldo, A., Fagherazzi, S., Lanzoni, S., Marani, M. and Dietrich, W.E. Tidal networks: 3.
772 Landscape-forming discharges and studies in empirical geomorphic
773 relationships. *Water Resources Research*, 35(12), pp.3919-3929, 1999.

774 Rogers, K.G., and Goodbred, S.L. Mass failures associated with the passage of a large tropical
775 cyclone over the Swatch of No Ground submarine canyon (Bay of Bengal): *Geology*,
776 38(11), pp.1051–1054, 2010.

777 Rogers, K.G., Goodbred Jr, S.L. and Mondal, D.R. Monsoon sedimentation on the ‘abandoned’
778 tide-influenced Ganges–Brahmaputra delta plain. *Estuarine, Coastal and Shelf*
779 *Science*, 131, pp.297-309, 2013.

780 Rogers, K.G., and Overeem, I. Doomed to drown? Sediment dynamics in the human-
781 controlled floodplains of the active Bengal Delta. *Elementa: Science of the*
782 *Anthropocene*, 6, p. 66, doi:10.1525/elementa.250, 2017.

783 Saha, M.K., and Khan, N. Changing profile of cyclones in the context of climate change and
784 adaptation strategies in Bangladesh. *Journal of Bangladesh Institute of Planners*, 7, pp.
785 63-78, 2014.

786 Sakib, M., Nihal, F., Haque, A., Rahman, M., & Ali, M. Sundarban as a Buffer against Storm
787 Surge Flooding. *World Journal of Engineering and Technology*, 3, 59–64, 2015.

788 Sarwar, M.G.M. and Woodroffe, C.D. Rates of shoreline change along the coast of
789 Bangladesh. *Journal of Coastal Conservation*, 17(3), pp.515-526, 2013.

790 Seijger, C., Datta, D.K., Douven, W., van Halsema, G. and Khan, M.F. Rethinking sediments,
791 tidal rivers and delta livelihoods: tidal river management as a strategic innovation in
792 Bangladesh. *Water Policy*, doi: <https://doi.org/10.2166/wp.2018.212>, 2018.

793 Shaha, D.C. and Cho, Y.K. Salt plug formation caused by decreased river discharge in a
794 multi-channel estuary. *Scientific Reports*, 6, p.27176, 2016.

795 Shampa, M., and Pramanik, I.M. Tidal River Management (TRM) for Selected Coastal Area of
796 Bangladesh to Mitigate Drainage Congestion. *International Journal of Scientific and
797 Technology Research*, 1(5), pp.1–6, 2012.

798 Steckler, M.S., Nooner, S.L., Akhter, S.H., Chowdhury, S.K., Bettadpur, S., Seeber, L. and
799 Kogan, M.G. Modeling Earth deformation from monsoonal flooding in Bangladesh using
800 hydrographic, GPS, and Gravity Recovery and Climate Experiment (GRACE)
801 data. *Journal of Geophysical Research: Solid Earth*, 115(B8), 2010.

802 Syvitski, J.P. Supply and flux of sediment along hydrological pathways: research for the 21st
803 century. *Global and Planetary Change*, 39(1-2), pp.1-11, 2003.

804 Syvitski, J.P. and Milliman, J.D. Geology, geography, and humans battle for dominance over
805 the delivery of fluvial sediment to the coastal ocean. *The Journal of Geology*, 115(1),
806 pp.1-19, 2007.

807 Syvitski, J.P. Deltas at risk. *Sustainability Science*, 3(1), pp.23-32, 2008.

808 Syvitski, J.P., Kettner, A.J., Overeem, I., Hutton, E.W., Hannon, M.T., Brakenridge, G.R., Day, J.,
809 Vörösmarty, C., Saito, Y., Giosan, L. and Nicholls, R.J. Sinking deltas due to human
810 activities. *Nature Geoscience*, 2(10), p.681, 2009.

811 Uddin, M. S., van Steveninck, E. D. R., Stuip, M., & Shah, M. A. R. Economic valuation of
812 provisioning and cultural services of a protected mangrove ecosystem: a case study on
813 Sundarbans Reserve Forest, Bangladesh. *Ecosystem Services*, 5, 88-93, 2013.

814 van Staveren, M.F., Warner, J.F., Khan, M.S.A., and Shah Alam Khan, M. Bringing in the tides.
815 From closing down to opening up delta polders via Tidal River Management in the
816 southwest delta of Bangladesh. *Water Policy*, 19(1), pp.147–164, 2016.

817 Wilson, C., Goodbred, S., Small, C., Gilligan, J., Sams, S., Mallick, B. and Hale, R. Widespread
818 infilling of tidal channels and navigable waterways in human-modified tidal delta plain
819 of southwest Bangladesh. *Elem Sci Anth*, 5, 2017.

820 Winterwerp, J.C. and Giardino, A. Assessment of increasing freshwater input on salinity and
821 sedimentation in the Gorai river system. *World Bank Project*, pp.1206292-000, 2012.

822 Yan, W. Can mangroves buffer ocean acidification?, *Eos*, 97, 2016.

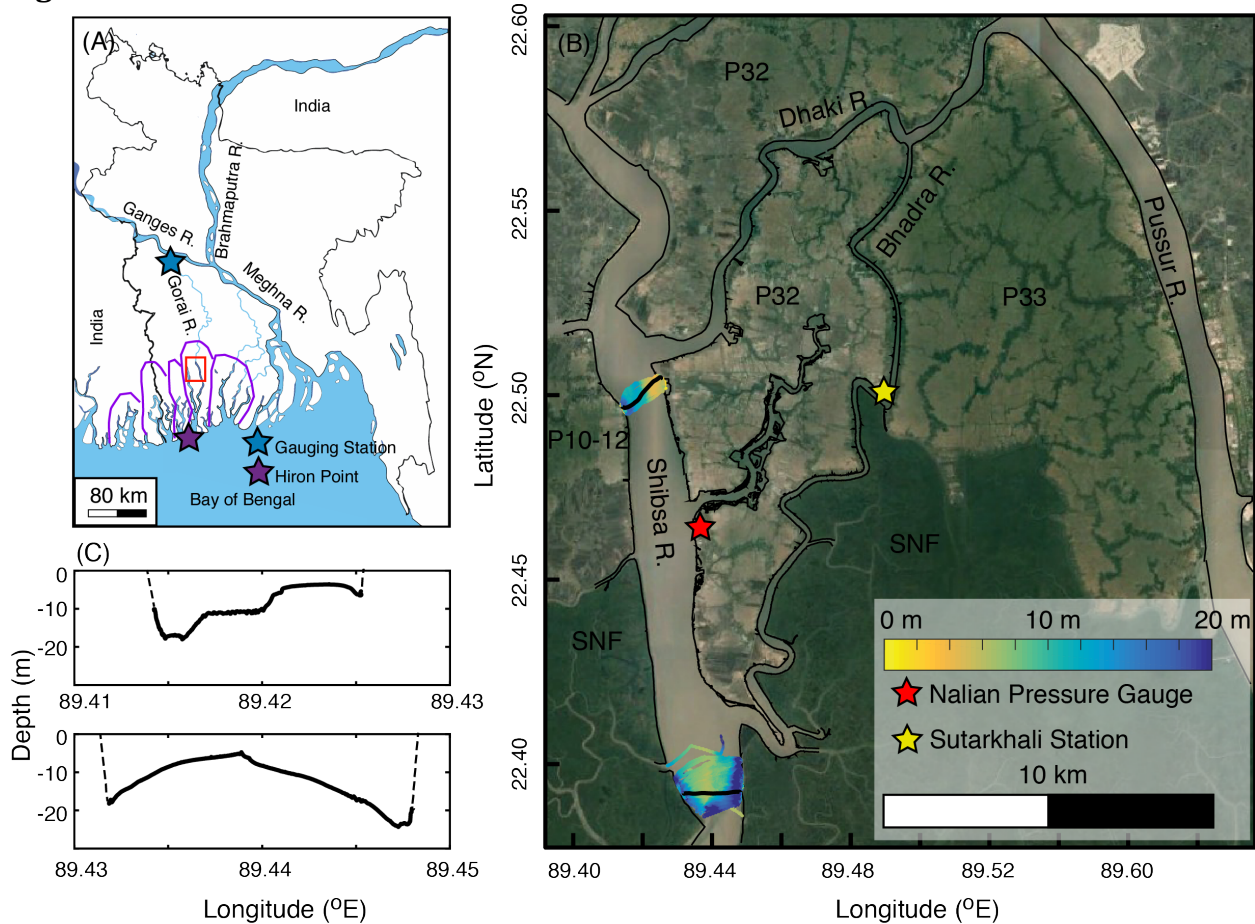
823
824
825
826
827

828 Table 1: Measurements of sediment flux and tidal prism from the Shibs River. Shaded
 829 rows represent measurements taken during spring tides.
 830

	Transect	Tidal Range (m)	Tidal Prism (m ³)			Sediment Load (kg)		
			Ebb	Flood	Net	Ebb	Flood	Net
Dry Season	South	2.1	2.00E+08	-2.00E+08	4.30E+05	2.05E+07	-4.70E+07	-2.66E+07
	North	2.2	1.40E+08	-1.50E+08	-1.30E+07	1.55E+07	-2.37E+07	-8.21E+06
	South	5.5	4.50E+08	-4.30E+08	2.30E+07	1.83E+08	-2.30E+08	-4.69E+07
	North	5.7	3.10E+08	-2.30E+08	7.90E+07	2.15E+08	-1.90E+08	2.49E+07
Monsoon	South	2.7	2.64E+08	-1.81E+08	8.28E+07	4.47E+07	-3.89E+07	5.77E+06
	North	2.2	1.83E+08	-1.06E+08	7.69E+07	6.20E+07	-4.12E+07	2.08E+07
	South	4	4.71E+08	-5.12E+08	-4.16E+07	3.20E+08	-3.85E+08	-6.50E+07
	North	3.9	2.40E+08	-2.85E+08	-4.43E+07	2.54E+08	-3.31E+08	-7.65E+07

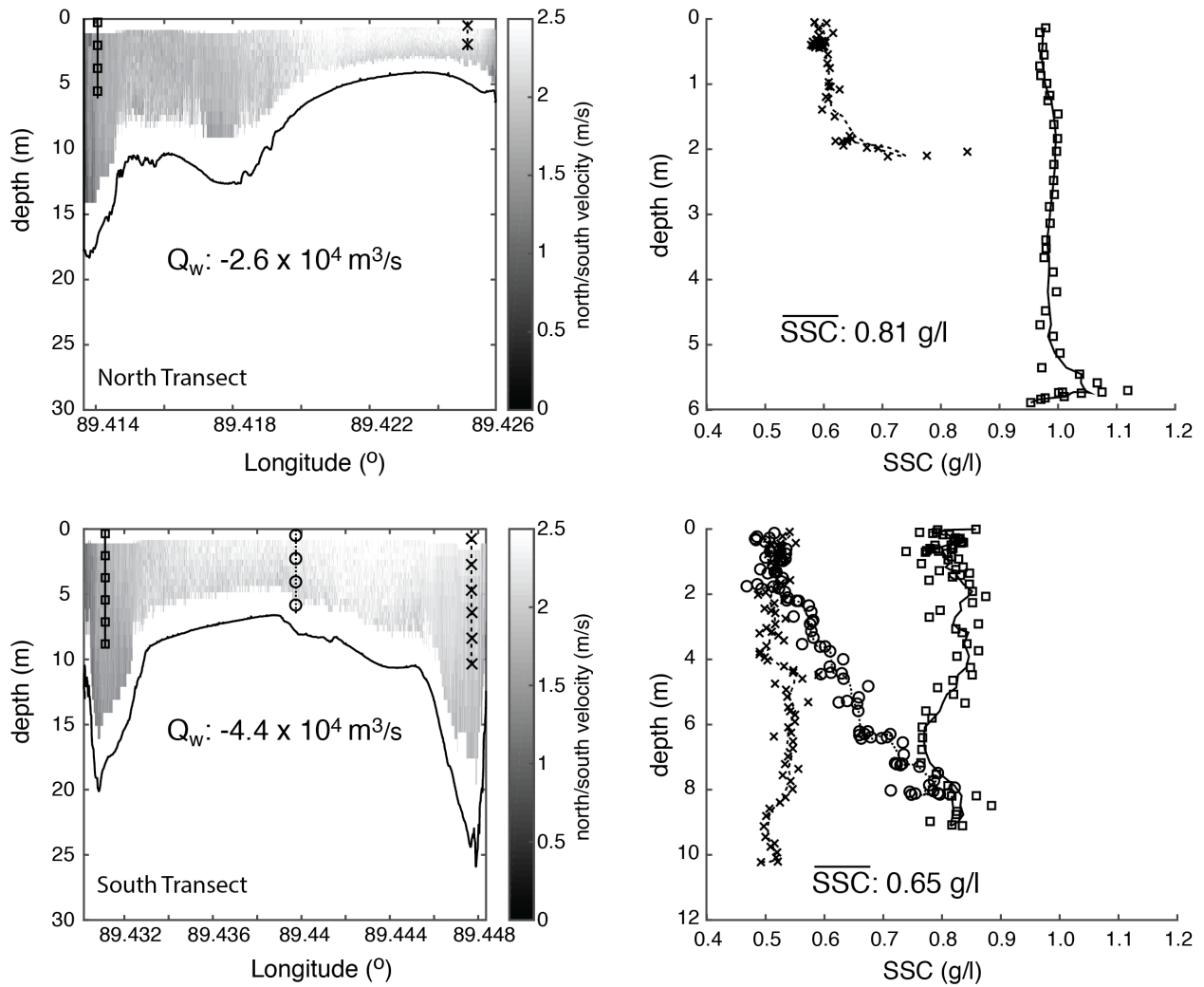
831
 832
 833

834 **Figures:**



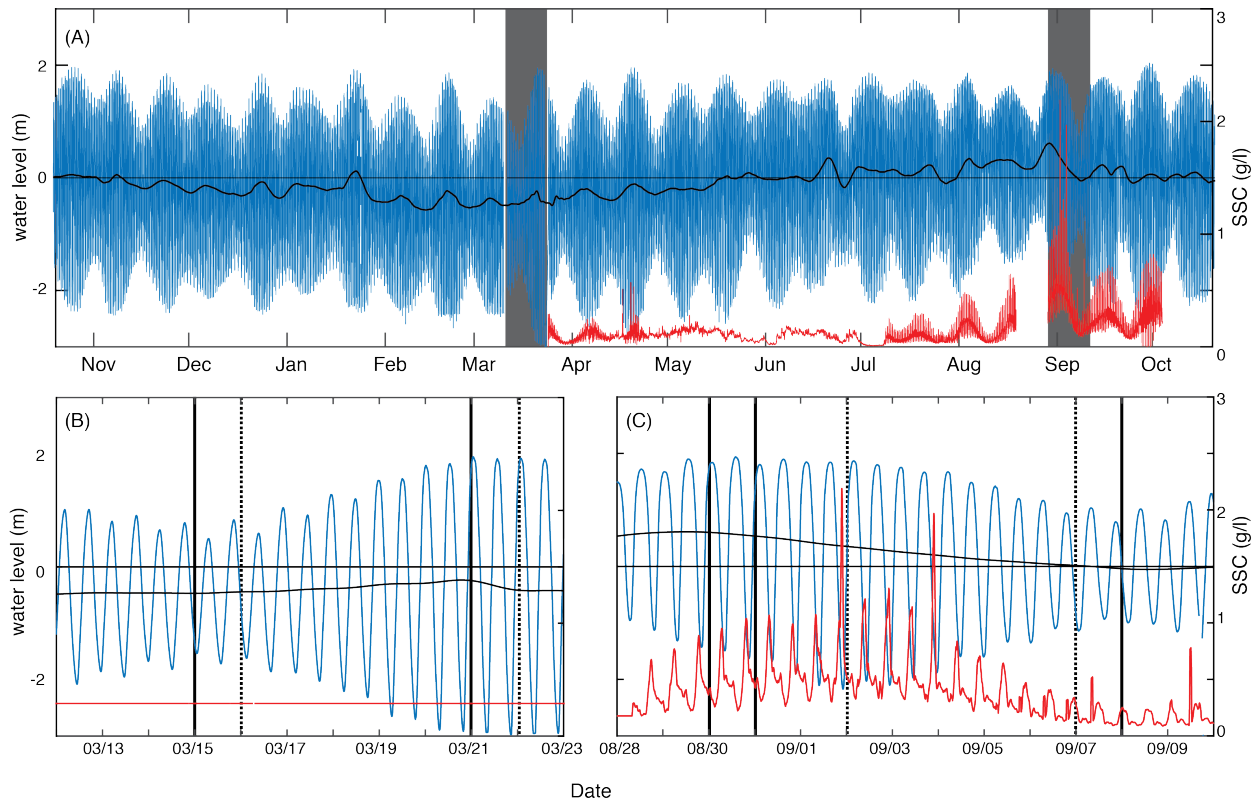
835
836
837
838
839
840
841
842

Fig. 1 – A) Location of Bangladesh and the specific region of interest for this study, as well as the approximate outlines of the five major tidal distributary basins of the SW delta in purple. B) Satellite image of P-32 study area, with bathymetry overlain in the regions of the northern and southern transects. Long-term and short-term pressure sensor locations are also identified. C) Characteristic river cross sections for the northern and southern transects. The specific transects used for these cross sections are highlighted in black in (B).

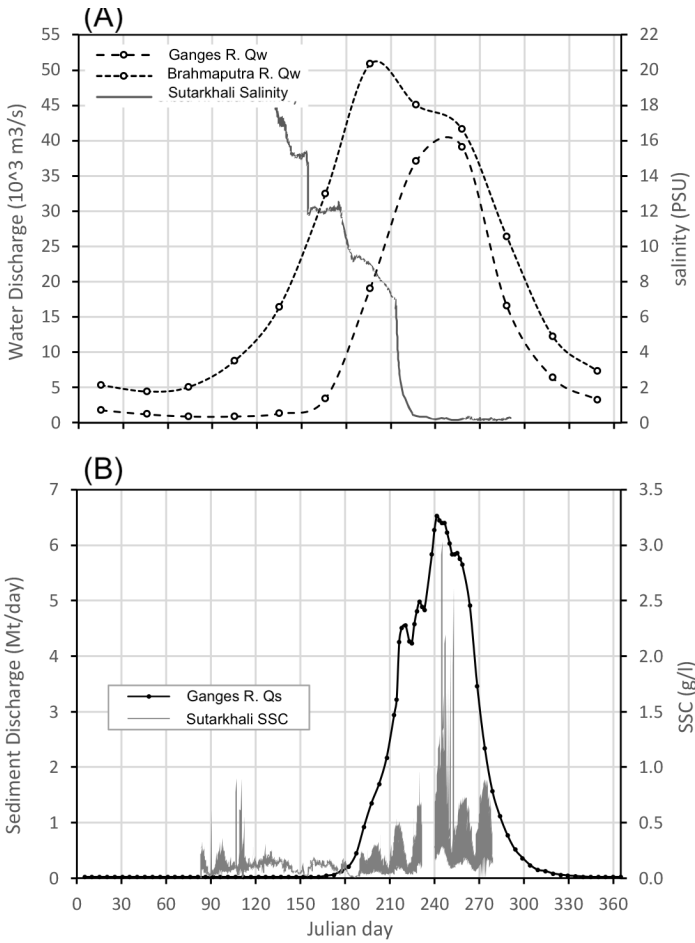


843
844
845
846
847

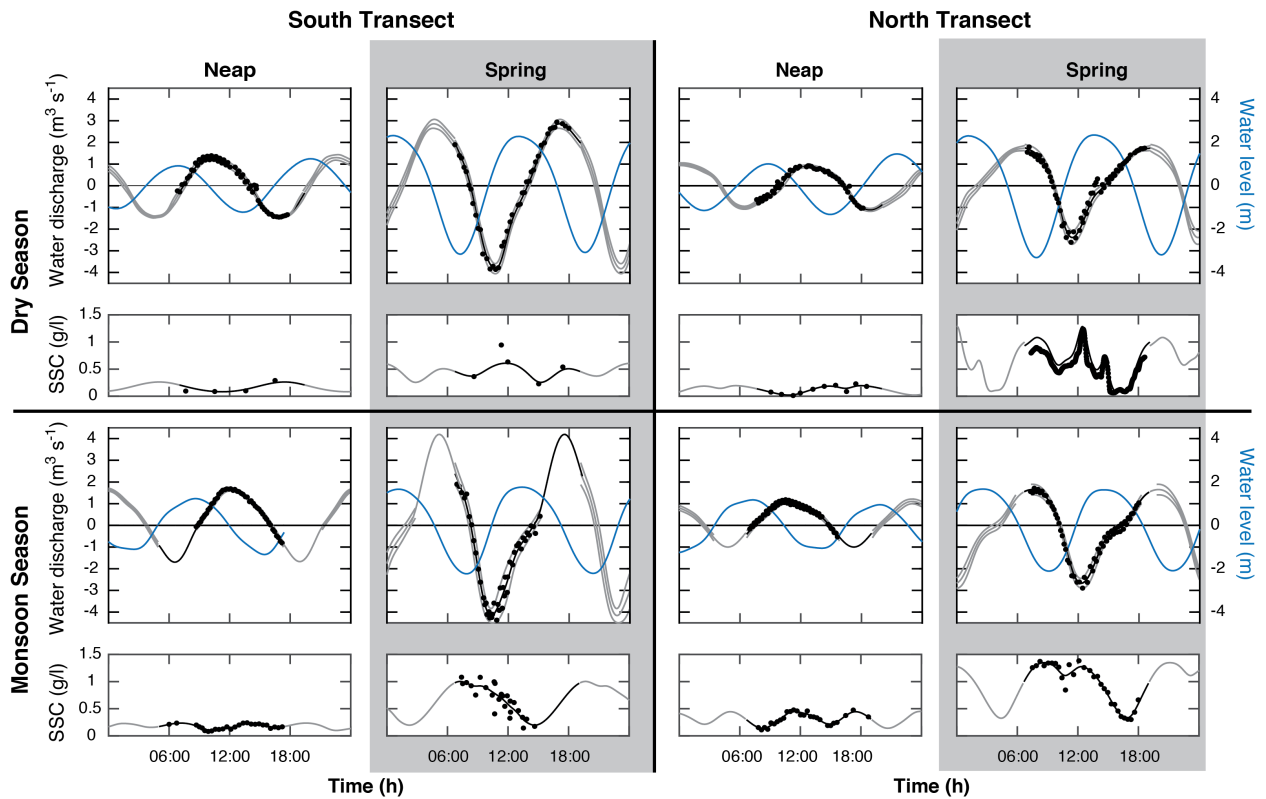
Fig. 2 – Example channel cross sections of velocity and SSC collected near maximum ebb-oriented tides during the wet season at the north (top) and south (bottom) transects. Velocity measurements are spatially integrated to compute water discharge. SSC are averaged, with the product of velocity and SSC used to compute sediment discharge.



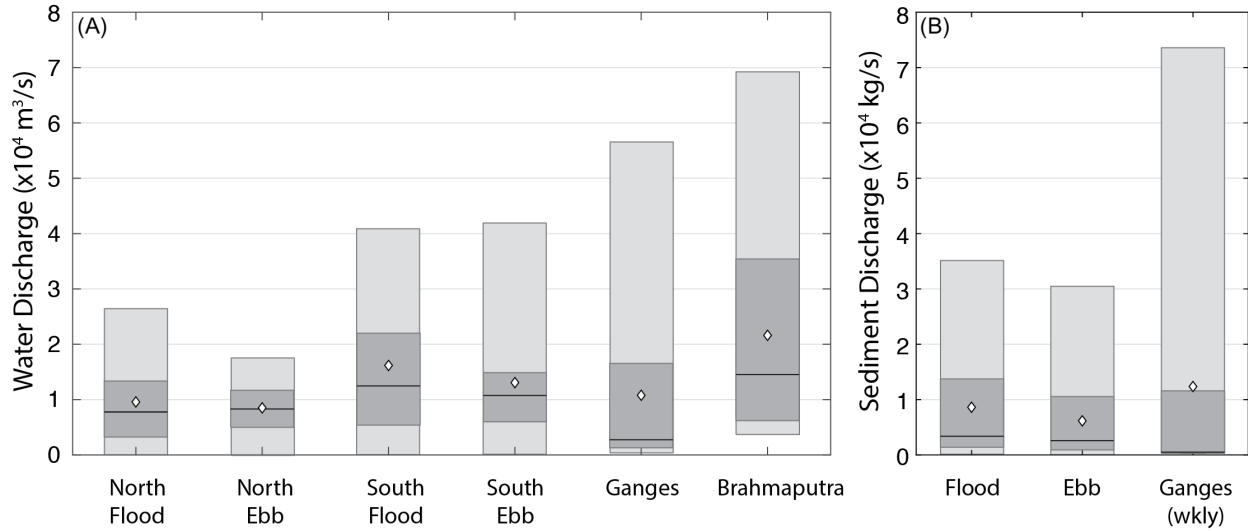
848
 849 Fig. 3 – A) Long-term water level elevation (blue) and suspended sediment concentration
 850 (red) recorded at Sutarkhali. Black is the tidally filtered water level to highlight seasonal
 851 trends of relatively higher water during the monsoon, despite similar maximum tidal
 852 elevation. Note also the arrival of increased SSC associated with monsoon discharge of the
 853 GBM, beginning in August. Areas shaded in gray depict the periods of focused field work,
 854 highlighted below in panels (B) and (C). Days where transect measurements were recorded
 855 are noted with vertical black lines, where solid are from the southern transect, and dashed
 856 are from the northern transect. In (B), the horizontal red line represents the maximum SSC
 857 observed in the spring-neap tidal cycle following our focused field work, as SSC was not
 858 measured at this location previously.



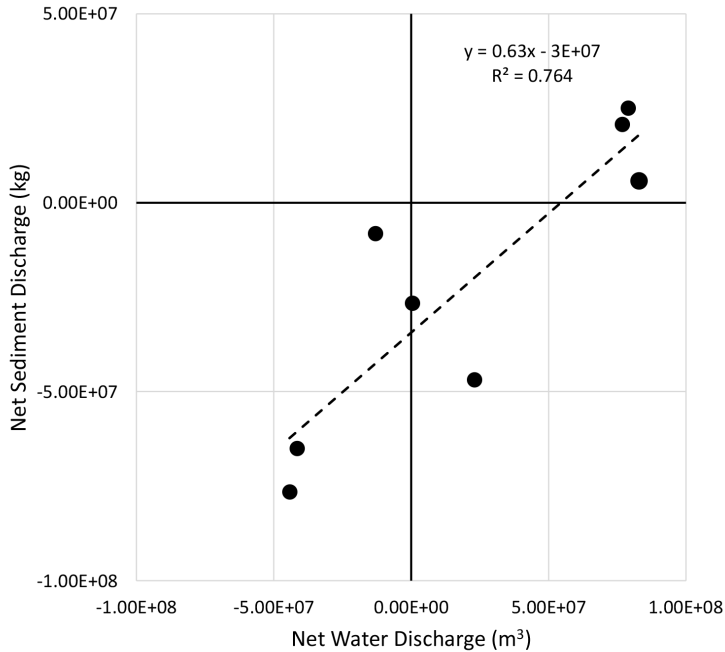
859
 860 Fig. 4 – A) Ganges and Brahmaputra River water discharge (Q_w), and salinity measured at
 861 Sutarkhali Station, demonstrating the reduction in P-32 salinity associated with the arrival
 862 of freshwater from the GBM rivers. B) Ganges river sediment discharge (Q_s) interpolated
 863 from Lupker et al. (2011) and SSC measured at Sutarkhali station, demonstrating the
 864 increase in local SSC coincident with the peak SSC discharge of the Ganges R.



865
 866 Fig. 5 – Instantaneous water discharge, water level, and depth and width-averaged SSC for
 867 each day of cross-channel transects. Dry season measurements are in the upper half, while
 868 monsoon season transects are on the bottom. Spring tides in either season are shaded in
 869 gray. The two left columns are southern measurements, and the two right columns are
 870 from the northern transect. Black dots correspond to specific measurements, while gray
 871 lines represent the estimated error, tile forwards and backwards by 12.4 hours. For
 872 discharge, dashed lines in the monsoon represent maxima based on extrapolations from
 873 the dry season ratio. While seemingly unreasonable, they are provided here for context.
 874
 875
 876



877
 878 Fig. 6 – Comparison of mean (diamond), median (black line), 25th and 75th percentile
 879 (lower and upper limits of darkly shaded box) and total range (lightly shaded box) for
 880 water discharge (A), and sediment discharge (B). A) demonstrates that median and mean
 881 discharge along either transect are comparable to those of either the Ganges or
 882 Brahmaputra River. B) demonstrates that as with water, mean sediment discharge on both
 883 the flood and ebb tides is approximately the same as the weekly averaged Ganges sediment
 884 discharge.



885
 886 Fig. 7 – Net water discharge vs. net sediment discharge for all of the survey days on the
 887 Shibsa River. As expected, we observe a positive trend to this relationship. The negative y-
 888 intercept of the best-fit curve demonstrates the overall flood-oriented nature of sediment
 889 transport in this tidal channel.